Article

Not peer-reviewed version

Ternary Holey Carbon nanohorns/KCl/PVP Nanohybrid As Sensing Film For Resistive Humidity Sensor

Bogdan-Catalin Serban *, Octavian Buiu *, Marius Bumbac *, Nicolae Dumbravescu, Cristina Pachiu, Mihai Brezeanu, Gabriel Craciun, Cristina Mihaela Nicolescu, Vlad Diaconescu, Cornel Cobianu

Posted Date: 8 March 2024

doi: 10.20944/preprints202403.0476.v1

Keywords: holey carbon nanohorns (CNHox); potassium chloride (KCl); polyvinylpyrrolidone (PVP); nanohybrid; resistive R.H. sensor

Article

Ternary Holey Carbon Nanohorns/KCl/PVP Nanohybrid as Sensing Film For Resistive Humidity Sensor

Bogdan-Catalin Serban [1,2,*], Octavian Buiu [1,2,*], Marius Bumbac [3,4,*], Nicolae Dumbravescu [1,2], Cristina Pachiu [1], Mihai Brezeanu [5], Gabriel Craciun [1], Cristina Mihaela Nicolescu [4], Vlad Diaconescu [5] and Cornel Cobianu [5,6]

[1] National Institute for Research and Development in Microtechnologies-IMT Bucharest, 126 A Erou Iancu Nicolae Str., 077190 Voluntari, Romania; bogdan.serban@imt.ro (B.C.S.) octavian.buiu@imt.ro (O.B.); nicolae.dumbravescu@imt.ro (N.D.); cristina.pachiu@imt.ro (C.P.);
[2] Research Center for Integrated Systems, Nanotechnologies, and Carbon-Based Nanomaterials (CENASIC) - I.M.T. Bucharest, Romania.
[3] Faculty of Sciences and Arts, Sciences and Advanced Technologies Department, Valahia University of Targoviste, 13 Sinaia Alley, 130004, Targoviste, Dambovita, Romania; marius.bumbac@valahia.ro (M.B.);
[4] Institute of Multidisciplinary Research for Science Technology, Valahia University of Targoviste, 13 Sinaia Alley, 130004, Targoviste, Dambovita Romania, cristina.nicolescu@valahia.ro (C.M.N.)
[5] National University of Science and Technology Politehnica Bucharest., 313 Splaiul Independentei., 060042, Bucharest, Romania; scriemiceva@hotmail.com (M.B.); cornel.cobianu@upb.ro (C.C.)
[6] Academy of Romanian Scientists (A.R.S.), Str. Ilfov Nr. 3, Sector 5, Bucharest, Romania, cornel.cobianu@upb.ro, (C.C.)
[7] University of Medicine and Pharmacy "Carol Davila," Dionisie Lupu Street, no. 37, Sector 2, Bucharest, diaconescuvld506@gmail.com, (V.D.)
* Correspondence: bogdan.serban@imt.ro; octavian.buiu@imt.ro; marius.bumbac@valahia.ro

Abstract: We report the relative humidity (R.H.) sensing response of a resistive sensor, employing sensing layers based on a ternary nanohybrid comprising holey carbon nanohorns (CNHox), potassium chloride (KCl), and polyvinylpyrrolidone (PVP) at mass ratios 7/1/2, 6.5/1.5/2, and 6/2/2 (w/w/w/w). The sensing structure comprises a silicon substrate, a SiO_2 layer, and interdigitated transducer (IDT) electrodes. The sensing film is deposited on the sensing structure via the drop-casting method. The sensing layers' morphology and composition are investigated through Scanning Electron Microscopy (S.E.M.) and RAMAN spectroscopy. The ternary hybrid-based thin film resistance increases when the sensors are exposed to R.H., ranging from 0% to 100%. The manufactured devices show a room temperature response comparable to a commercial capacitive R.H. sensor and are characterized by excellent linearity, rapid response time, and good sensitivity. The presented sensors exhibit superior performance in terms of sensitivity compared to other similarly manufactured and tested sensors that employ a CNHox-based sensing layer. We explain the sensing role of each constituent of the ternary hybrid nanocomposites based on their chemical and physical properties, electronic properties, and affinity for water molecules. Different alternative sensing mechanisms are considered and discussed, such as the decreasing number of holes in the holey CNHox at the interaction with water molecules, proton conduction, and PVP swelling.

Keywords: holey carbon nanohorns (CNHox); potassium chloride (KCl); polyvinylpyrrolidone (PVP); nanohybrid; resistive R.H. sensor

1. Introduction

Humidity is an important environmental variable that plays a significant role in daily life. Consequently, humidity monitoring has become an essential issue in a large variety of residential, industrial, and commercial applications such as controlling and sensing humidity in offices and homes for human comfort, medical field (gas supply infrastructure, respiration monitoring, incubators, infusion pumps, ventilators, sterilizers), pharmaceutical industry (packaging, storage), food/beverage quality monitoring, cosmetics. Furthermore, the utilization of R.H. sensors is vital in

 doi:10.20944/preprints202403.0476.v1

electronic manufacturing (semiconductor fabrication plants), the chemical industry (dehumidifiers, dryers), metallurgy, the textile and paper industry, agriculture (soil moisture detection), climatology, textile and paper industry, automotive industry (engine tests beds), etc. [1–5]. Therefore, the R.H. sensors market has experienced substantial growth in the last decades [6], and it is expected to reach an overall value of more than 8,7 bn USD by 2029 [7]. Within this market, the family of resistive R.H. sensors has several advantages, making them the preferred choice when addressing specific requirements of the applications translated into: a. cost-effective, b. a more straightforward design, c. a wider operating range, d. a fast response time and e. low power consumption. These advantages come with some limitations – lower accuracy and stability, a non-linear response, and a shorter lifespan – among the most important ones.

Apart from the sensing principle (electrochemical, optical, gravimetric, capacitive, piezoresistive, or resistive), fabrication technologies, and sensor design, the materials selected as the sensing layer appear critical in developing R.H. sensors with superior performances [8]. So far, several materials have been investigated as sensing layers within the design of humidity sensors: mesoporous silica [9], CdS [10], macroporous silicon [11], metal oxide semiconductors [12–14], ceramics [15] conducting polymers [16,17], polyelectrolytes [18], porphirins [19], black phosphorus [20], 2D MXene [21].

Moreover, many carbon–based materials are extensively used as sensing layers within the design of the R.H. sensors. Their large specific surface area, ability to work at room temperature, high mechanical strength, high chemical inertness, and facile hydrophilization of carbonic film through covalent functionalization make these materials interesting candidates for sensitive coatings for resistive humidity monitoring. Carbon nanofibers [22], carbon nanosheets [22], carbon mesoporous [24], amorphous carbon [25], carbon dots [26], N- doped hydrogenated amorphous carbon [27], nanodiamond [28], carbon nanocoil [29], carbon nanotubes and their nanocomposites [30], graphene oxide [31], reduced graphene oxide [32], fullerenol [33], and fullerenes [34] are some of the carbonic nanomaterials studied for R.H. sensing applications.

In particular, thanks to their outstanding physical, chemical, and electrical properties, CNHs-based materials have been widely used for R.H. sensing applications in the last few years. Several types of C.N.H.s and their nanocomposites were used as sensing layers within the design of chemoresistive R.H. sensors: pristine C.N.H.s [35], oxidized carbon nanohorns (CNHox) [36], binary nanocomposites, such as CNHs-PVP [37], CNHox-PVP [38], CNHox-poly(ethylene glycol)-block-poly(propylene glycol)-block-poly(ethylene glycol) [38] and ternary nanocomposites, such as GO-CNHox–PVP [39]. Furthermore, several nanohybrids, such as CNHox/SnO_2/ZnO/PVP [40], CNHox)/TiO_2/PVP [8], and CNHox/ ZnO/PVP [41], were also used as sensing layers for R.H. resistive monitoring. Last but not least, alkali ions, such as K^+ [42–45], Li^+[46,47], or Na^+[48], were often used in fabricating R.H. sensors as dopants to improve the sensing parameters.

This paper presents the R.H. sensing response of a resistive sensor employing a sensing layer based on a ternary nanohybrid comprising CNHox/KCl/PVP at mass ratios 7/1/2, 6.5/1.5/2, and 6/2/2 (w/w/w/w). The study emphasizes the R.H. sensing capabilities of the newly CNHox–based nanohybrid operating at room temperature (R.T.).

2. Materials and Methods

2.1. Materials

All the materials used in the R.H. measurements were purchased from Sigma Aldrich (Redox Lab Supplies Com, Bucharest, Romania). Holey CNHox, with the structure shown in Figure 1a, is characterized by lengths between 40 nm and 50 nm, diameters between 2 nm and 5 nm, and a specific surface area of around 1300-1400 m^2/g. According to the supplier, CNHox used in experiments has no metal contamination, and graphite is the main impurity (around 10 % w/w). The PVP employed has the structure depicted in Figure 1b and an average molar weight of 40,000 g mol-1. The KCl used in the experiments has 99,99 % purity (with impurities ≤15.0 ppm - trace metal analysis). Isopropyl

 doi:10.20944/preprints202403.0476.v1

alcohol ($(CH_3)_2CHOH$) is a solution 70 % w/w in water. All reagents were used as received without further purification.

(**a**) (**b**)

Figure 1. The structure of (**a**) holey CNHox, (**b**) PVP.

2.2. Preparation of the Quaternary Organic-Inorganic Holey CNH-Based Hybrid Sensing Films and Experimental Setup

For the investigation of the R.H. sensing capabilities of the ternary nanohybrid, the following chemical compositions of the sensing films were designed, synthesized, and tested: CNHox/KCl/PVP=7/1/2, CNHox/KCl/PVP=6.5/1.5/2, CNHox/KCl/PVP=6/2/2, all being expressed as mass ratios (w/w/w/w). The mixture was homogenized in isopropyl alcohol using a mild sonication bath (FS20D Fisher Scientific, Dreieich, Germany), working at 42 kHz (output power of 70 W). This process provides a relatively uniform dispersion of the CNHox and KCl in the PVP network.

The synthesis of the sensing films based on CNHox, KCl, and PVP with different weight ratios was performed by applying a five-step procedure. First, the PVP solution was prepared by dissolving 2 mg hydrophilic polymer in 10 mL isopropyl alcohol under stirring in the ultrasonic bath for 10 minutes. Then, a holey CNHox (7 mg, 6,5 mg, and 6 mg, respectively) was dispersed in the previously manufactured PVP solution and stirred in the ultrasonic bath for 6 hours at R.T. Afterward, KCl powder was added to the resulting suspension according to the desired mass ratios (1 mg, 1.5 mg, and 2 mg KCl), and a continuous stirring was performed in the ultrasound bath for another 6 hours, also at R.T. In the end, the sensing layer was obtained by the drop-casting method, depositing the annealed mixture on the support structure, while its electrical contact areas were masked before the addition of the sensing dispersion. All samples were dried at 373 K for 60 minutes before electrical measurements were performed.

The sensing support structure consists of a metallic interdigitated electrodes (IDE) dual-comb structure fabricated on a Si substrate (470 μm thickness), covered by a SiO_2 layer (1 μm thickness) (Figure 2). The metal stripes of the IDE comprise chromium (10 nm thickness) and gold (100 nm thickness) [39–41,49].

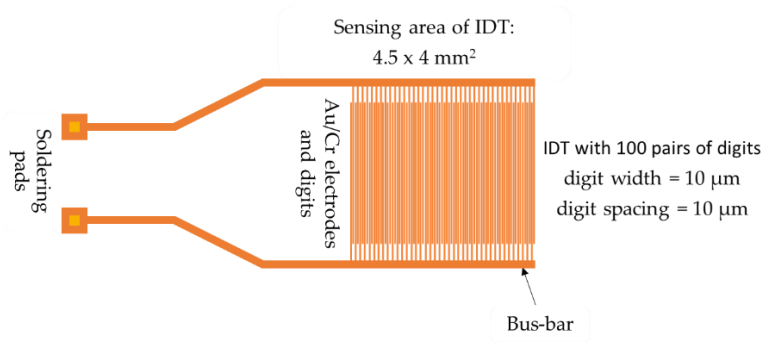

Figure 2. The layout of the IDE sensing structure.

 doi:10.20944/preprints202403.0476.v1

The R.H. monitoring tests were performed in an appropriate experimental setup (Figure 3). The dry nitrogen was injected through recipients arranged in series containing deionized water (conductivity below 1 μS/cm) so that a controlled variation of the R.H. in the testing chamber was obtained from 0 % to 100 % R.H.. The testing chamber included two sensors: one capacitive R.H. commercial sensor (C.O.M.) as reference and the new resistive sensing structure (abbreviated as S.U.I. – "sensor under investigation"), having as sensing layers the nanocomposite mixtures of CNHox/KCl/PVP at different w/w/w ratios. The roles of the reference sensor (C.O.M.) were, on the one hand, to validate the R.H. level indicated by the mass flow controller and, on the other hand, to provide an objective comparison of the data measured on the S.U.I. Positioning the two sensors near each other and close to the gas inlet was ensured to expose them to identical gas flow and quasi-similar experimental conditions.

A Keithley 6620 current source (Keithley Instruments GmbH, Germering, Germany) provided a direct current variation between 0.01 – 0.1 A. The data were collected and analyzed with a PicoLog data logger (PICO Technology, Neots, Cambridgeshire, United Kingdom). All the measurements were performed at R.T.

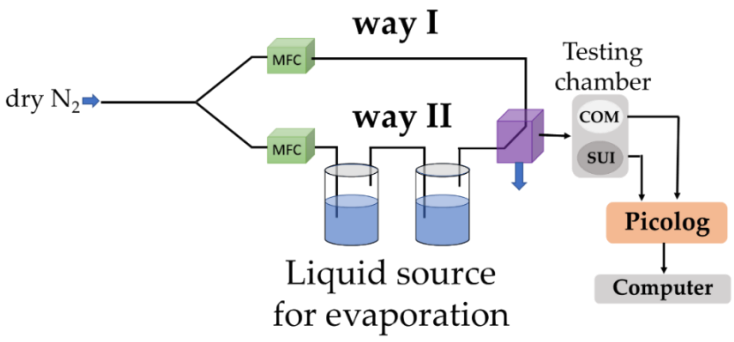

Figure 3. Experimental setup employed for R.H. measurements.

The R.H. sensing capability of each ternary nanohybrid–based sensing layer was explored by applying a current between the two electrodes and measuring the voltage difference when varying the R.H. from 0% to 100%. To simplify the analysis, the following abbreviations will be used:

- Sensor K1 is the resistive sensor that employs a sensing layer based on CNHox/KCl/PVP at a 7/1/2 mass ratio.
- Sensor K2 is the resistive sensor that employs a sensing layer based on CNHox/KCl/PVP at a 6.5/1.5/2 mass ratio.
- Sensor K3 is the resistive sensor that employs a sensing layer based on CNHox/KCl/PVP at a 6/2/2 mass ratio.

The Raman spectra have been collected at R.T. with a Witec Raman spectrometer (Alpha-SNOM 300 S, WiTec. GmbH, Germany) using 532 nm as an excitation. The 532-nm diode-pumped solid-state laser has a maximum power of 145 mW. The incident laser beam with a spot size of about 1.0 μm was focused onto the sample with 6 mm working distance objective attached to a Thorlabs MY100X-806 microscope. The Raman spectra were measured with an exposure time of 20 s accumulation, and the scattered light was collected by the same objective in back-scattering geometry with 600 grooves/mm grating. The calibration of the Raman systems was carried out using the 520-cm−1 Raman line of a silicon wafer. The spectrometer scanning data collection and processing were done by a dedicated computer using WiTec Project Five software.

Scanning electron microscopy (S.E.M.) investigated the sensing films' surface topography. A field emission gun scanning electron microscope, FEG-SEM-Nova NanoSEM 630 (Thermo Scientific, Waltham, MA, U.S.A.) (F.E.I.), was used for surface visualization with superior low voltage resolution and high surface sensitivity imaging. The samples were investigated directly (i.e., no sample preparation was needed). The current during the measurements was 1 nA.

 doi:10.20944/preprints202403.0476.v1

Atomic force microscopy (A.F.M.) analysis was performed using Witec alpha 300S Gmbh Germany system in tapping mode with a Si_3N_4 A.F.M. cantilever (125 µm long, force constant of 40 N/m and frequency 300 kHz). The surface parameters were calculated using Project FIVE 5.0 Witec software.

3. Results

3.1. Surface Topography

Scanning electron micrographs show that the surface morphology of the coating mixture is relatively homogenous in all the cases (Figures 4–6). At the same time, particles of much larger dimensions (> 100 nm) can be observed due to the aggregation of particles of various sizes and crystallographic orientations.

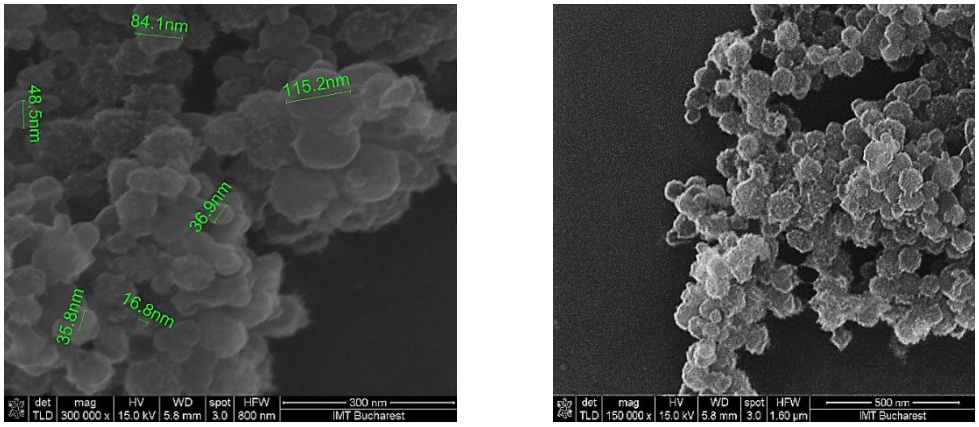

(**a**) (**b**)

Figure 4. SEM of the K1′ sensing layer at: (**a**) x 300,000 magnification; (**b**) x 150,000 magnification.

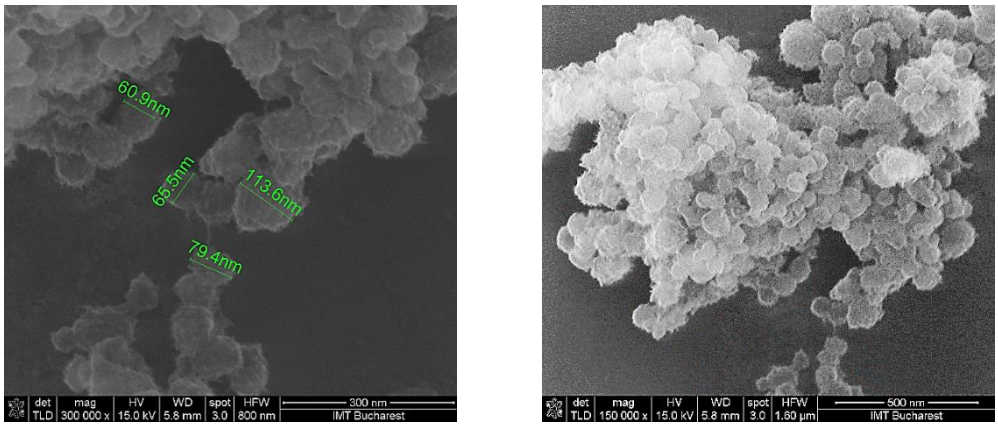

(**a**) (**b**)

Figure 5. SEM of the K2′ sensing layer at: (**a**) x 300,000 magnification; (**b**) x 150,000 magnification.

Preprints.org (www.preprints.org) | NOT PEER-REVIEWED | Posted: 8 March 2024 doi:10.20944/preprints202403.0476.v1

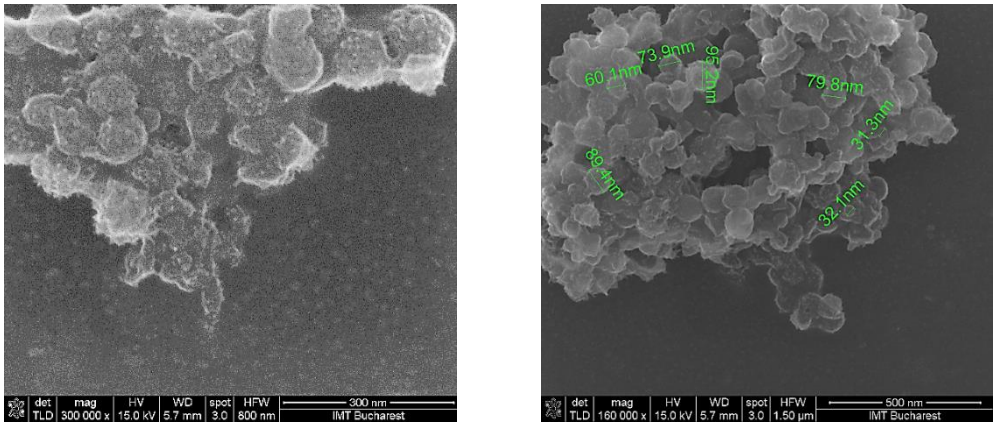

(**a**) (**b**)

Figure 6. SEM of the K3′ sensing layer at: (**a**) x 300,000 magnification; (**b**) x 160,000 magnification.

3.2. Raman Spectroscopy

The Raman spectra of the ternary nanohybrids CNHox/KCl/PVP are presented in Figure 7a–c. In Figure 7d, spectra p1-p3 are three acquisition points per sample (sample K3). In the p2 (grey) and p3 (black) spectra, between 0-1000 cm^{-1} are the vibration modes of Si combined with PVP, and above 2700 cm^{-1} is a vibration mode specific to PVP. Blue spectrum is pure PVP spectrum. The Raman spectrum of powder PVP, for wavelengths below 1000 cm-1, includes vibration lines associated with groups N-C=O (560 cm^{-1}) and C-C (758 cm^{-1}, 851 cm^{-1}, and 934 cm^{-1})

It can be observed that three active Raman bands (D, G, 2D) were recorded at the wavenumbers of 1,332, 1,587, and 2,660 cm^{-1}, which are typical for sp^2-defected carbon nanomaterials. According to the Raman spectrum of pure PVP, the weak band at 2990 cm^{-1} can be attributed to PVP [50].

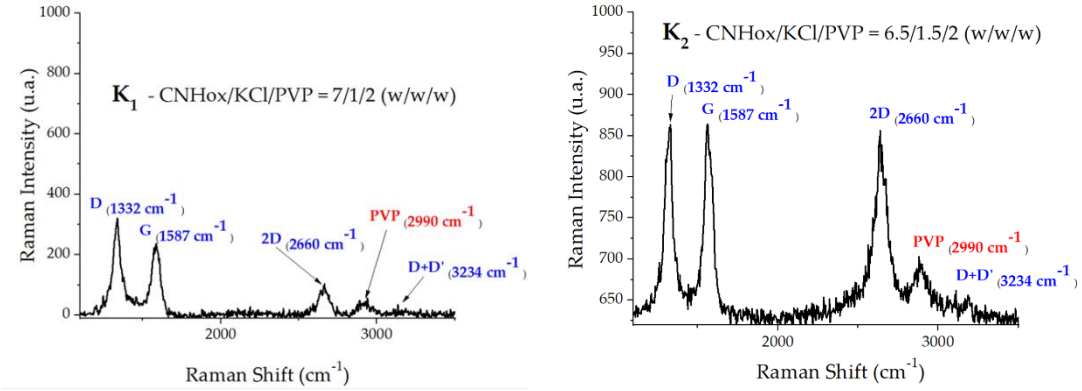

(**a**) (**b**)

Preprints.org (www.preprints.org) | NOT PEER-REVIEWED | Posted: 8 March 2024 doi:10.20944/preprints202403.0476.v1

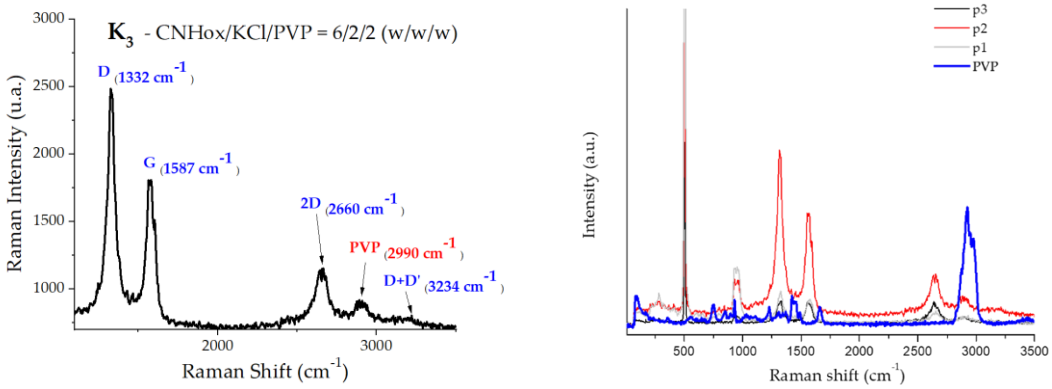

(**c**) (**d**)

Figure 7. Raman spectra of ternary nanocomposite CNHox/KCl/PVP.

3.3. R.H. Monitoring Capability of the Ternary Nanocomposite

The present R.T. resistive R.H. sensor has an organic-inorganic sensitive layer containing oxidated carbon nanohorn (CNHox) with a concentration higher than the percolation threshold of the solid-state nanocomposite [55]. This chemical design of the nanocarbonic component assured a reasonably low value of the electrical conductivity of the sensing layer and simple, functional device measurability.

The R.H. sensor response of the manufactured sensors is presented in Figures 8–10. As shown in Figures 8–10, the resistance of the ternary nanohybrid-based thin film increases when R.H. increases. A notable characteristic of these sensors is their low power consumption, below 2 mW.

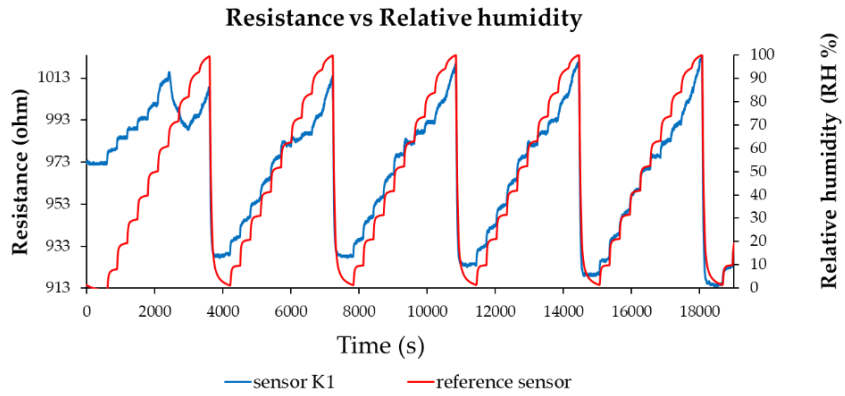

Figure 8. Resistance versus R.H. for the K1 sensor in several operating sequences.

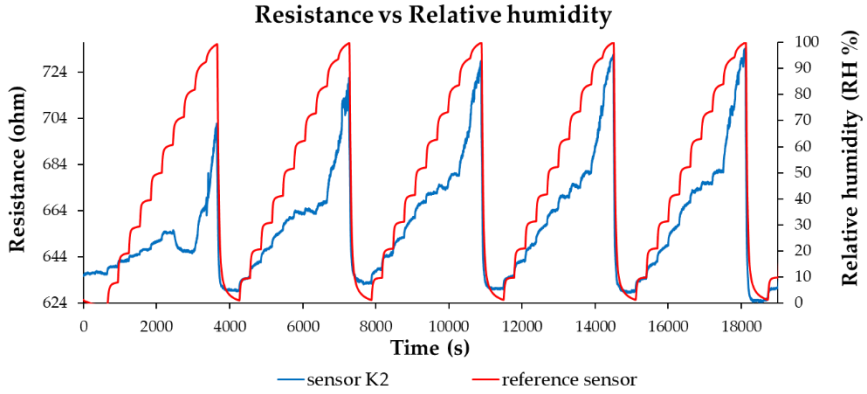

Preprints.org (www.preprints.org) | NOT PEER-REVIEWED | Posted: 8 March 2024 doi:10.20944/preprints202403.0476.v1

Figure 9. Resistance versus R.H. for the K2 sensor in several operating sequences.

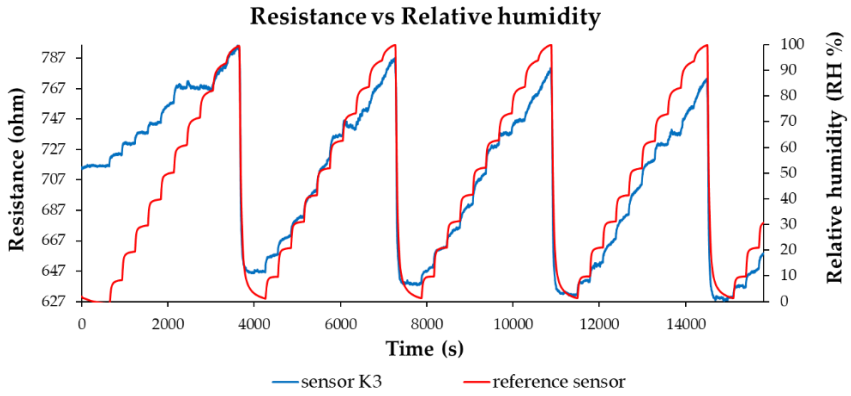

Figure 10. Resistance versus relative humidity for the K3 sensor in several operating sequences.

At the same time, the overall linearity of the ternary nanohybrid-based resistive sensors—in humid nitrogen when varying R.H. from 0% to 100%—is excellent, as shown in Figure 11. In terms of linearity, all the manufactured sensors show superior performances ($R^2 > 0.99$) for operating cycles 2-6 and an excellent baseline drift, but for R.H., values up to 80%. It is interesting to note a different behavior in the first operating cycle compared to other operating cycles. At R.H. higher than 80%, a sharp increase in resistance with R.H. can be observed.

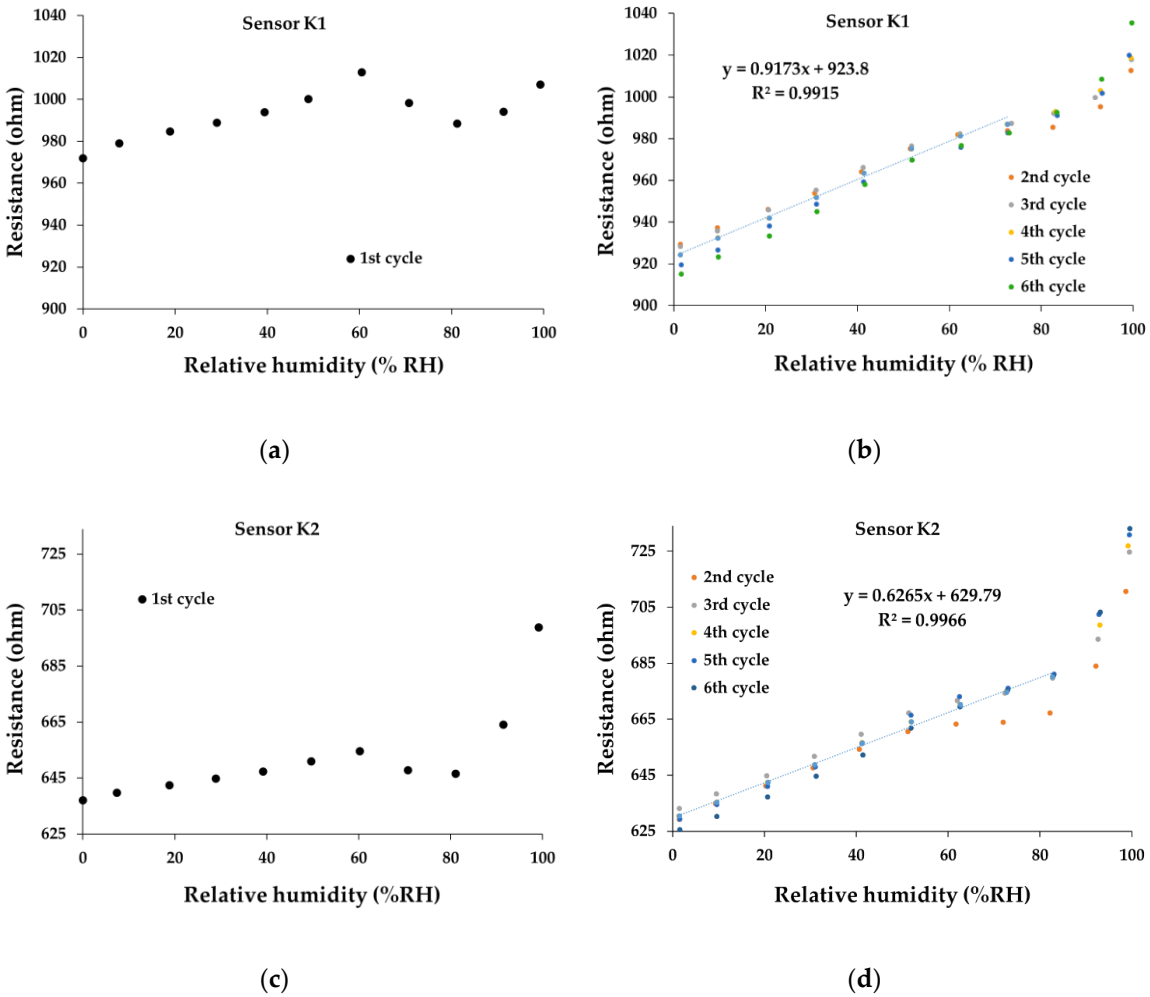

Preprints.org (www.preprints.org) | NOT PEER-REVIEWED | Posted: 8 March 2024 doi:10.20944/preprints202403.0476.v1

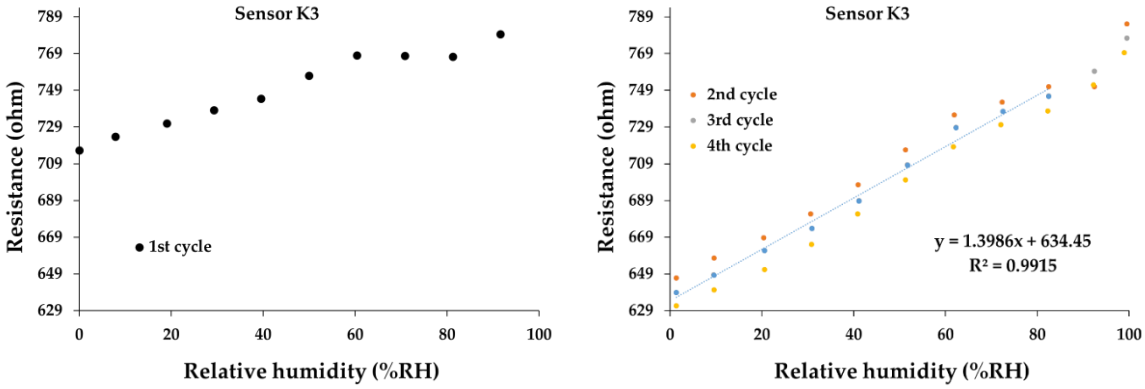

(**e**) (**f**)

Figure 11. The transfer function of the sensor: (**a**) K1 – 1st cycle, (**b**) K1- 2nd to 6th cycles, (**c**) K2 – 1st cycle, (**d**) K2- 2nd to 6th cycles, (**e**) K3 – 1st Cycle, (**f**) K3 - 2nd to 6th cycles in humid nitrogen (RH = 0%- 100%).

Figure 11e,f present the transfer function for the sensor K3. It is noticeable that after the first cycle, there is a reduction in the resistance at R.H.=0, from 710-715 Ω to 630-635 Ω. The same behavior is registered also for the sensor K1 (Figure 11a,b), with a decrease of resistance (for R.H.=0) from 970 Ω (first cycle) to 910 Ω and 930 Ω (subsequent cycles).

The calculation of sensitivity was made using the equation:

$$S = \frac{\Delta R_x}{\Delta RH_x} = \frac{R_x - R_0}{RH_x}, \quad (1)$$

where: Rx is the resistance of the sensitive layer measured in the test chamber for the [x - %] R.H. value indicated by the commercial sensor (measured with ± 2% accuracy as the producer indicates it). R_0 is the value of resistance calculated from the linear function established from the graph of resistance = f (relative humidity) by extrapolation for the value at 0% R.H. The calculated relative sensitivity values for each humidity jump are presented in Figure 12a–c.

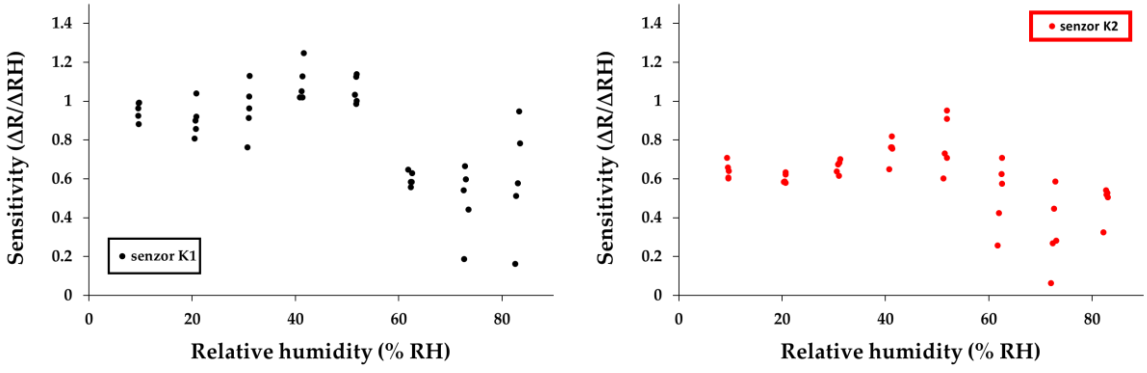

(**a**) (**b**)

Preprints.org (www.preprints.org) | NOT PEER-REVIEWED | Posted: 8 March 2024 doi:10.20944/preprints202403.0476.v1

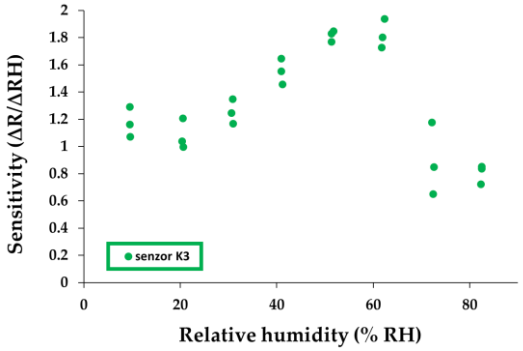

(**c**)

Figure 12. Sensitivity calculated for each humidity jump for sensors: (**a**) K1, (**b**) K2, and (**c**) K3 in humid nitrogen (R.H. = 0%- 90%);.

A simple comparison between the calculated sensitivities for K1, K2, and K3 sensors and other similarly manufactured and tested sensors that employed holey CNHOx–based sensing layers reveals interesting results (Table 1). As one can see, K1, K2, and K3 sensors exhibit superior performances in terms of sensitivity in comparison with other reported sensors. The high hydrophilicity of the alkali salt has a significant contribution, increasing the number of active sites towards water molecules. In addition, the enhanced sensing layer porosity and its associated high specific surface area can also contribute to this result.

Table 1. Comparison between different CNHox-based RH sensing layers and sensing performances for similarly manufactured and tested sensors.

Sensing layer (mass ratio)	Sensitivity ($S = \frac{\Delta R}{\Delta RH}$) (Ω/%RH)	Reference
CNHox	0.013-0.021	[35]
CNHox/PVP 1/1	0.020-0.058	[37]
CNHox/PVP 1/2	0.017-0.025	[37]
CNHox/GO/PVP 3/1/1	0,043-0, 051	[38]
CNHox/GO/ SnO2/ PVP 0.75/0.75/1/1	0.548–0.770	[49]
CNHox/G.O./SnO2/PVP 1/1/1/1	0.798–0.980	[49]
CNHox/KCl/PVP 7/1/2 (K1)	0.200–1.245	This work
CNHox/KCl/PVP 6.5/1.5/2 (K2)	0.300-0.950	This work
CNHox/KCl/PVP 6/2/2 (K3)	0.650-1.940	This work

An important parameter, such as response time (t_r), was calculated for all manufactured R.H. resistive sensors. If R(t) is the response of the device in time, t_r can be calculated as:

$$t_r = t_{90} - t_{10}, \quad (2)$$

where t_{90} and t_{10} represent the moments when the response R(t) reaches 90% and 10%, respectively, from the total variation of the sensor's resistance due to a change in the R.H. value (as in the example presented in Figure 13).

Preprints.org (www.preprints.org) | NOT PEER-REVIEWED | Posted: 8 March 2024 doi:10.20944/preprints202403.0476.v1

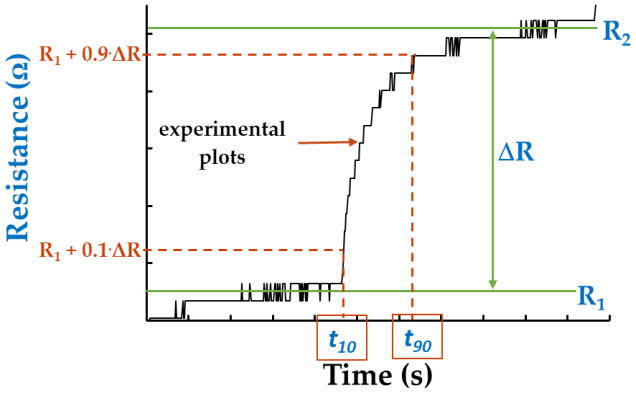

Figure 13. Example of calculating the response time.

Figure 14 presents graphical representations of the ratios between the response time of the investigated sensors and that of the reference sensor (C.O.M.) calculated for each R.H. jump: a) K1, b) K2, and c) K3 in humid nitrogen (R.H. = 0%- 100

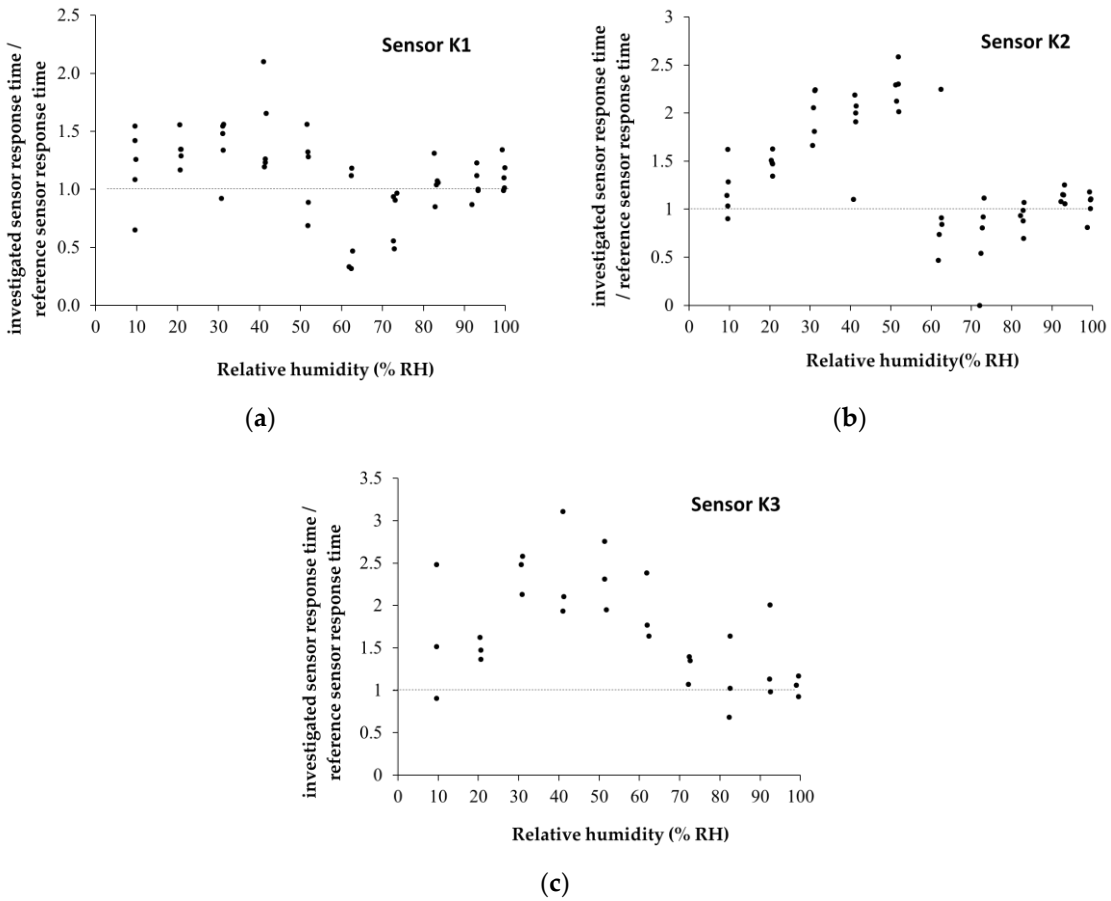

Figure 14. Graphical representations of the ratios between the response time of investigated sensors and the response time of C.O.M. calculated for each humidity jump: (**a**) K1, (**b**) K2, and (**c**) K3 in humid nitrogen (R.H. = 0%- 100%).

The reference sensor has a response time of 60 s +/- 10 s for R.H. below 70%. The response time for R.H.> 70% increases to approximately 90 s +/-10 s. Water molecules permeate the hydrophilic nanohybrid sensing film. The hybrid nanocomposite film adsorbs/absorbs a substantial amount of

 doi:10.20944/preprints202403.0476.v1

water (related to the sensing film's mass). Finally, some water molecules can condense in the proximity of hydrophilic groups, thus blocking the active sites.

4. Analysis of the Sensing Mechanism

All constituents of the ternary nanohybrid used as a sensing layer in resistive monitoring of R.H. have some outstanding chemical and physical properties. CNHox shows increased conductivity (p-type semiconductor behavior), a remarkable and controllable surface area (1300 to 1400 m^2/g), high porosity, hydrophilicity, as well as a rapid variation of the electrical resistance in contact with a water molecule in the 0% R.H. to 100% R.H. range. Furthermore, low-cost synthesis of CNHox via oxygen plasma treatment of the pristine C.N.H.s is a simple, clean, and fast procedure. Last but not least, the functionalization of the C.N.H.s in oxygen plasma has the advantage (by varying the exposure time as well as its power) that it can provide an optimal C:O ratio for superior sensitivity towards water molecules [51].

At the same time, PVP is a hydrophilic polymer with excellent binding and dispersion properties. The addition of alkali ions. such as K^+, ensures more active sites for water molecules.

Given the attributes of the above-mentioned constituents of the sensing layer, three distinct sensing mechanisms are considered. The first analysis is related to the p-type semiconducting behavior of the CNHox. When interacting with the CNHox, the water molecules donate their electron pairs, thus decreasing the number of positive charge carriers (holes) in the nanocarbonic material. Therefore, the humidity-sensing film becomes more resistive. Several reviews reported in the literature confirm this interpretation [52].

The second sensing mechanism considers the dissociation of water. Due to the strong electrostatic field and high local charge density, the adsorbed water molecules on the CNHox hydrophilic surface and mesopores may dissociate to H^+ and $O.H.^-$ ions. The protons generated by the water dissociation process may tunnel from one water molecule to another through hydrogen bonding, thus increasing the overall electrical conductivity of the sensitive film [53].

PVP is a dielectric polymer with hydrophilic properties, which swells after interaction with water molecules and has a negligible change in resistance in response to R.H. variation, as shown in literature for the presented composites [54–56]. Based on these properties, a third sensing mechanism can be discussed. The swelling of PVP leads to the displacement of CNHox, increases the distance between nanocarbon particles, and lowers the number of electrically percolating pathways. Accordingly, the device resistance increases upon exposure to a higher level of R.H. because more water molecules penetrate the bulk of the sensing layer.

Finally, the contribution of KCl to the sensing mechanism can be interpreted from two perspectives. Firstly, according to the Hard-Soft Acid Base (HSAB) theory, the K+ ion is classified as a hard acid and can electrostatically interact with water molecules, which are classified as hard bases (electron donors) [57,58]. Thus, adding potassium salt can provide more active sites for humidity, increasing the local concentration of water molecules in the sensing layer. Due to the p-type semiconducting behavior of CNHox and the PVP swelling, a higher number of water molecules leads to a significant increase in resistance. At the same time, once the local concentration of water molecules increases, KCl is dissolved, the ions can move freely, and the conductivity of the sensing layer increases.

In conclusion, as described above, the interaction of the sensing layer with water molecules has, theoretically, antagonistic effects on its resistance variation. Since the measured resistance of the sensing film increases when R.H. increases from 0% to 100%, one can assume that the cumulative effect of the p-type semiconductor behavior of the CNHox and the swelling of PVP is the dominant cause that leads. Therefore, without completely excluding the impact of both the proton-tunneling mechanism and ionic conduction through K+ and Cl- ions, the interaction of the CNHox-PVP tandem with water has a pivotal contribution to the variation of the resistance of the sensing layer with R.H.

As one can see, for all studied sensing layers, the thin film's resistance decreases after the first operating cycle of the sensor. The higher the percentage of KCl in the sensitive layer, the more

 doi:10.20944/preprints202403.0476.v1

significant the decrease in resistance. This experimental result agrees with the idea that the ionic conduction mechanism is predominant in the first operating cycle.

5. Conclusions

In this study, the R.H. sensing response of an R.H. detection structure employing, as a sensing layer, a ternary nanohybrid comprising holey CNHox (with concentration levels above the percolation threshold), KCl, and PVP at mass ratios 7/1/2, 6.5/1.5/2, and 6/2/2 (w/w/w/w), were reported.

The sensing structure comprises a silicon substrate, a SiO_2 layer, and an IDE. The sensing film was deposited on the sensing structure via the drop-casting method. The sensing layers' morphology and composition were investigated through S.E.M. and RAMAN spectroscopy. The manufactured sensors showed good room temperature response comparable to a commercial capacitive R.H. sensor. They were characterized by excellent linearity, rapid response, and good sensitivity. At the same time, they exhibited superior performances in terms of sensitivity in comparison with other similarly manufactured and tested sensors that employed holey CNHox–based sensing layers.

The role of each component of the ternary nanohybrid used as sensing film was explained based on their electrical, chemical, and physical properties. Three distinct sensing mechanism types were considered and discussed. Based on the sensing results, the *p*-type semiconductor behavior of CNHox, in conjunction with the swelling of the hydrophilic polymer used (PVP), was shown to prevail and lead to the overall increase of the resistance of the sensing films with R.H. for all the manufactured sensors.

The low power consumption of the manufactured sensors, below 2 mW, their sensing performances at room temperature, and their manufacturing simplicity are the essential benefits of the presented sensors.

6. Patents

Bogdan-Catalin Serban, Octavian Buiu, Marius Bumbac, Cristina Mihaela Nicolescu, Nanohibrid ternar pentru monitorizarea rezistiva a umiditatii relative, Romanian patent Application, The official bulletin of industrial property, OSIM, 137854A2, 29.12.2023.

Author Contributions: Conceptualization, Bogdan-Catalin Serban, Octavian Buiu and Cornel Cobianu; Formal analysis, Bogdan-Catalin Serban, Octavian Buiu, Cristina Pachiu, Vlad Diaconescu and Cornel Cobianu; Funding acquisition, Octavian Buiu and Marius Bumbac; Investigation, Bogdan-Catalin Serban, Octavian Buiu, Nicolae Dumbravescu, Cristina Pachiu and Gabriel Craciun; Methodology, Bogdan-Catalin Serban, Octavian Buiu, Nicolae Dumbravescu, Cristina Pachiu and Cornel Cobianu; Project administration, Bogdan-Catalin Serban and Octavian Buiu; Resources, Octavian Buiu, Marius Bumbac and Cristina Mihaela Nicolescu; Software, Marius Bumbac, Mihai Brezeanu and Cristina Mihaela Nicolescu; Supervision, Octavian Buiu; Validation, Bogdan-Catalin Serban, Octavian Buiu, Nicolae Dumbravescu, Cristina Pachiu, Mihai Brezeanu, Vlad Diaconescu and Cornel Cobianu; Visualization, Nicolae Dumbravescu and Cristina Pachiu; Writing – original draft, Bogdan-Catalin Serban, Octavian Buiu, Marius Bumbac, Nicolae Dumbravescu, Cristina Pachiu, Mihai Brezeanu, Gabriel Craciun, Cristina Mihaela Nicolescu and Cornel Cobianu; Writing – review & editing, Bogdan-Catalin Serban, Octavian Buiu, Marius Bumbac, Cristina Pachiu, Mihai Brezeanu, Gabriel Craciun and Vlad Diaconescu.

Funding: The authors would like to acknowledge the financial support provided by the Romanian Ministry of Research and Education, via the "Nucleu Program" called MICRO-NANO-SIS PLUS", grant number P.N. 19 16.

Institutional Review Board Statement: Not applicable.

Informed Consent Statement: Not applicable.

Data Availability Statement: Not applicable.

Conflicts of Interest: The authors declare no conflict of interest.

 doi:10.20944/preprints202403.0476.v1

References

1. Ma, Z., Fei, T., & Zhang, T. (2023). An overview: Sensors for low humidity detection. *Sensors and Actuators B: Chemical*, *376*, 133039.
2. Ku, C. A., & Chung, C. K. (2023). Advances in Humidity Nanosensors and Their Application. *Sensors*, *23*(4), 2328.
3. Huang, C., Jiang, M., & Liu, F. (2023). Recent Progress on Environmentally Friendly Humidity Sensor: A Mini Review. *A.C.S. Applied Electronic Materials*, *5*(8), 4067-4079.
4. Farhan, K. Z., Shihata, A. S., Anwar, M. I., & Demirboğa, R. (2023). Temperature and humidity sensor technology for concrete health assessment: a review. *Innovative Infrastructure Solutions*, *8*(10), 276.
5. Kumar, A., Gupta, G., Bapna, K., & Shivagan, D. D. (2023). Semiconductor-metal-oxide-based nanocomposites for humidity sensing applications. *Materials Research Bulletin*, *158*, 112053.
6. Barmpakos, D., & Kaltsas, G. (2021). A review on humidity, temperature and strain printed sensors—Current trends and future perspectives. *Sensors*, *21*(3), 739.
7. Global Humidity Sensor Market - Industry Trends and Forecast to 2029, https://www.databridgemarketresearch.com/reports/global-humidity-sensor-market, accessed February 2024.
8. Chen, Z., & Lu, C. (2005). Humidity sensors: a review of materials and mechanisms. *Sensor letters*, *3*(4), 274-295.
9. Tu, J., Li, N., Geng, W., Wang, R., Lai, X., Cao, Y., ... & Qiu, S. (2012). Study on a type of mesoporous silica humidity sensing material. *Sensors and Actuators B: Chemical*, *166*, 658-664.
10. Bhattacharjee, M., & Bandyopadhyay, D. (2019). Mechanisms of humidity sensing on a CdS nanoparticle coated paper sensor. *Sensors and Actuators A: Physical*, *285*, 241-247.
11. Wang, Y., Park, S., Yeow, J. T., Langner, A., & Müller, F. (2010). A capacitive humidity sensor based on ordered macroporous silicon with thin film surface coating. *Sensors and Actuators B: Chemical*, *149*(1), 136-142.
12. Li, P., & Yang, F. (2023). Preparation and performance of TiO2/ZnO humidity sensor based on TiO2. *Materials Science and Engineering: B*, *298*, 116902.
13. Kumar, A., Kumari, P., Kumar, M. S., Gupta, G., Shivagan, D. D., & Bapna, K. (2023). SnO2 nanostructured thin film as humidity sensor and its application in breath monitoring. *Ceramics International*.
14. Li, P., & Yang, F. (2023). Preparation and performance of TiO2/ZnO humidity sensor based on TiO2. *Materials Science and Engineering: B*, *298*, 116902.
15. Yao, J., Wang, J., Cao, W., Li, L., Luo, M., & Wang, C. (2023). Humidity Sensing Properties of (In+ Nb) Doped HfO2 Ceramics. *Nanomaterials*, *13*(5), 951.
16. Yang, Y., Wang, J., Lou, J., Yao, H., & Zhao, C. (2023). Fast response humidity sensor based on hyperbranched zwitterionic polymer for respiratory monitoring and non-contact human machine interface. *Chemical Engineering Journal*, *471*, 144582.
17. Memon, M. M., Hongyuan, Y., Pan, S., Wang, T., & Zhang, W. (2022). Surface Acoustic Wave Humidity Sensor Based on Hydrophobic Polymer Film. *Journal of Electronic Materials*, *51*(10), 5627-5634.
18. Dong, W., Ma, Z., & Duan, Q. (2018). Preparation of stable crosslinked polyelectrolyte and the application for humidity sensing. *Sensors and Actuators B: Chemical*, *272*, 14-20.
19. Rimeika, R., Čiplys, D., Poderys, V., Rotomskis, R., Balakauskas, S., & Shur, M. S. (2007). Subsecond-response S.A.W. humidity sensor with porphyrin nanostructure deposited on bare and metallised piezoelectric substrate. *Electronics Letters*, *43*(19), 1055-1057.
20. Yasaei, P., Behranginia, A., Foroozan, T., Asadi, M., Kim, K., Khalili-Araghi, F., & Salehi-Khojin, A. (2015). Stable and selective humidity sensing using stacked black phosphorus flakes. *ACS nano*, *9*(10), 9898-9905.
21. Haq, Y. U., Ullah, R., Mazhar, S., Khattak, R., Qarni, A. A., Haq, Z. U., & Amin, S. (2022). Synthesis and characterization of 2D MXene: Device fabrication for humidity sensing. *Journal of Science: Advanced Materials and Devices*, *7*(1), 100390.
22. Monereo, O., Claramunt, S., de Marigorta, M. M., Boix, M., Leghrib, R., Prades, J. D., ... & Cirera, A. (2013). Flexible sensor based on carbon nanofibers with multifunctional sensing features. *Talanta*, *107*, 239-247.
23. Chu, J., Peng, X., Feng, P., Sheng, Y., & Zhang, J. (2013). Study of humidity sensors based on nanostructured carbon films produced by physical vapor deposition. *Sensors and Actuators B: Chemical*, *178*, 508-513.
24. Sharath Kumar, J., Murmu, N. C., & Kuila, T. (2020). Recent Advances in Functionalized Micro and Mesoporous Carbon Nanostructures for Humidity Sensors. *Functional Nanomaterials: Advances in Gas Sensing Technologies*, 349-381.
25. Duan, Z., Yuan, Z., Jiang, Y., Liu, Y., & Tai, H. (2023). Amorphous carbon material of daily carbon ink: Emerging applications in pressure, strain, and humidity sensors. *Journal of Materials Chemistry C*.
26. Rivadeneyra, A., Salmeron, J. F., Murru, F., Lapresta-Fernández, A., Rodríguez, N., Capitan-Vallvey, L. F., ... & Salinas-Castillo, A. (2020). Carbon dots as sensing layer for printed humidity and temperature sensors. *Nanomaterials*, *10*(12), 2446.

 doi:10.20944/preprints202403.0476.v1

27. Frattini, G., Torres, S., Silva, L. I., Repetto, C. E., Gómez, B., & Dobry, A. (2021). The effect of nitriding on the humidity sensing properties of hydrogenated amorphous carbon films. *Physica Scripta*, *96*(5), 055701.
28. Yu, X., Chen, X., Yu, X., Chen, X., Ding, X., & Zhao, X. (2019). Flexible wearable humidity sensor based on nanodiamond with fast response. *IEEE Transactions on Electron Devices*, *66*(4), 1911-1916.
29. Wu, J., Sun, Y. M., Wu, Z., Li, X., Wang, N., Tao, K., & Wang, G. P. (2019). Carbon nanocoil-based fast-response and flexible humidity sensor for multifunctional applications. *A.C.S. applied materials & interfaces*, *11*(4), 4242-4251.
30. Chen, W. P., Zhao, Z. G., Liu, X. W., Zhang, Z. X., & Suo, C. G. (2009). A capacitive humidity sensor based on multi-wall carbon nanotubes (MWCNTs). *Sensors*, *9*(9), 7431-7444.
31. Tripathi, D., Tripathi, S., Rawat, R. K., & Chauhan, P. (2023). Highly Sensitive Humidity Sensor Based on Freestanding Graphene Oxide Sheets for Respiration and Moisture Detection. *Journal of Electronic Materials*, *52*(4), 2396-2408.
32. Liang, T., Hou, W., Ji, J., & Huang, Y. (2023). Wrinkled reduced graphene oxide humidity sensor with fast response/recovery and flexibility for respiratory monitoring. *Sensors and Actuators A: Physical*, *350*, 114104.
33. Wu, X., Wu, H., Jin, F., Ge, H. L., Gao, F., Wu, Q., ... & Yang, H. (2023). Facile preparation of fullerenol-based humidity sensor with highly fast response. *Fullerenes, Nanotubes and Carbon Nanostructures*, *31*(12), 1132-1136.
34. Li, X., Chen, X., Yu, X., Chen, X., Ding, X., & Zhao, X. (2017). A high-sensitive humidity sensor based on water-soluble composite material of fullerene and graphene oxide. *IEEE Sensors Journal*, *18*(3), 962-966.
35. Selvam, K. P., Nakagawa, T., Marui, T., Inoue, H., Nishikawa, T., & Hayashi, Y. (2020). Synthesis of solvent-free conductive and flexible cellulose–carbon nanohorn sheets and their application as a water vapor sensor. *Materials Research Express*, *7*(5), 056402.
36. Serban, B. C., Buiu, O., Dumbravescu, N., Cobianu, C., Avramescu, V., Brezeanu, M., ... & Nicolescu, C. M. (2020). Oxidized Carbon Nanohorns as Novel Sensing Layer for Resistive Humidity Sensor. *Acta Chimica Slovenica*, *67*(2).
37. Serban, B.C., Buiu O, Dumbravescu N., Avramescu V., Brezeanu M., Marinescu M.R., Bumbac M., Nicolescu C., EMERGEMAT, 5th International Conference, Emerging technologies in Engineering Materials, Bucharest, Romania, book of abstract, pg.90, 2022
38. Serban, B. C., Buiu, O., Dumbravescu, N., Cobianu, C., Avramescu, V., Brezeanu, M., ... & Nicolescu, C. M., Oxidized carbon nanohorn-hydrophilic polymer nanocomposite as the resistive sensing layer for relative humidity. *Analytical Letters*, **54**(3), 2021, 527-540.
39. Serban, B. C., Cobianu, C., Buiu, O., Bumbac, M., Dumbravescu, N., Avramescu, V., ... & Radulescu, C., Ternary nanocomposites based on oxidized carbon nanohorns as sensing layers for room temperature resistive humidity sensing. *Materials*, **14**(11), 2021, 2705.
40. Serban, B. C., Cobianu, C., Buiu, O., Bumbac, M., Dumbravescu, N., Avramescu, V., ... & Comanescu, F. C., Quaternary Holey Carbon Nanohorns/SnO2/ZnO/PVP Nano-Hybrid as Sensing Element for Resistive-Type Humidity Sensor, *Coatings*, **11**(11), 2021, 1307.
41. Serban, B. C., Buiu, O., Bumbac, M., Dumbravescu, N., Avramescu, V., Brezeanu, M., ... & Comanescu, F., Ternary Holey Carbon Nanohorns/TiO2/PVP Nanohybrids as Sensing Films for Resistive Humidity Sensors, *Coatings*, **11**(9), 2021, 1065.
42. Song, X., Qi, Q., Zhang, T., & Wang, C. (2009). A humidity sensor based on KCl-doped SnO2 nanofibers. *Sensors and Actuators B: Chemical*, *138*(1), 368-373.
43. Qi, Q., Zhang, T., Wang, S., & Zheng, X. (2009). Humidity sensing properties of KCl-doped ZnO nanofibers with super-rapid response and recovery. *Sensors and Actuators B: Chemical*, *137*(2), 649-655.
44. Geng, W., Yuan, Q., Jiang, X., Tu, J., Duan, L., Gu, J., & Zhang, Q. (2012). Humidity sensing mechanism of mesoporous MgO/KCl–SiO2 composites analyzed by complex impedance spectra and bode diagrams. *Sensors and Actuators B: Chemical*, *174*, 513-520.
45. Kunchakara, S., Dutt, M., Ratan, A., Shah, J., Singh, V., & Kotnala, R. K. (2019). Synthesis and characterizations of highly ordered KCl–MCM–41 porous nanocomposites for impedimetric humidity sensing. *Journal of Porous Materials*, *26*, 389-398.
46. Wang, W., Li, Z., Liu, L., Zhang, H., Zheng, W., Wang, Y., ... & Wang, C. (2009). Humidity sensor based on LiCl-doped ZnO electrospun nanofibers. *Sensors and Actuators B: Chemical*, *141*(2), 404-409.
47. Buvailo, A. I., Xing, Y., Hines, J., Dollahon, N., & Borguet, E. (2011). TiO2/LiCl-based nanostructured thin film for humidity sensor applications. *A.C.S. applied materials & interfaces*, *3*(2), 528-533.
48. Jiang, Y., Duan, Z., Fan, Z., Yao, P., Yuan, Z., Jiang, Y., ... & Tai, H. (2023). Power generation humidity sensor based on NaCl/halloysite nanotubes for respiratory patterns monitoring. *Sensors and Actuators B: Chemical*, *380*, 133396.
49. Serban, B. C., Cobianu, C., Buiu, O., Bumbac, M., Dumbravescu, N., Avramescu, V., ... & Comanescu, F. (2021). Quaternary Oxidized Carbon Nanohorns—Based Nanohybrid as Sensing Coating for Room Temperature Resistive Humidity Monitoring. *Coatings*, *11*(5), 53

 doi:10.20944/preprints202403.0476.v1

50. Heidari, B., Salmani, S., Sasani Ghamsari, M., Ahmadi, M., & Majles-Ara, M. H. (2020). Ag/PVP nanocomposite thin film with giant optical nonlinearity. *Optical and Quantum Electronics*, *52*, 1-18.
51. Le, G. T., Lerkprasertkun, P., Sano, N., Wu, K. C. W., & Charinpanitkul, T. (2023). Carbon nanohorns with surface functionalized by plasma treatment and their applications in drug delivery systems. *Journal of Science: Advanced Materials and Devices*, *8*(3), 100616.
52. Santra, S., Hu, G., Howe, R. C. T., De Luca, A., Ali, S. Z., Udrea, F., ... & Hasan, T. (2015). CMOS integration of inkjet-printed graphene for humidity sensing. *Scientific reports*, *5*(1), 17374
53. Borini, S.; White, R.; Wei, D.; Astley, M.; Haque, S.; Spigone, E.; Harris, N.; Kivioja, J.; Ryhanen, T. Ultrafast graphene oxide humidity sensors. ACS Nano 2013, 7, 11166–11173. Therefore, the humidity sensing film should become less resistive.
54. Li, B.; Weng, X.; Sun, X.; Zhang, Y.; Lv, X.; Gu, G. Facile synthesis of Fe3O4/reduced graphene oxide/polyvinyl pyrrolidone ternary composites and their enhanced microwave absorbing properties. J. Saudi Chem. Soc. 2018, 22, 979–984.
55. Serban, B. C., Cobianu, C., Dumbravescu, N., Buiu, O., Bumbac, M., Nicolescu, C. M., ... & Serbanescu, M. (2021). Electrical percolation threshold and size effects in polyvinylpyrrolidone-oxidized single-wall carbon nanohorn nanocomposite: The impact for relative humidity resistive sensors design. *Sensors*, *21*(4), 1435.
56. Serban, B. C., Cobianu, C., Dumbravescu, N., Buiu, O., Avramescu, V., Bumbac, M., ... & Brezeanu, M. (2020, October). Electrical percolation threshold in oxidized single wall carbon nanohorn-polyvinylpyrrolidone nanocomposite: A possible application for high sensitivity resistive humidity sensor. In *2020 International Semiconductor Conference (C.A.S.)* (pp. 239-242). IEEE.
57. Serban, B., Kumar, A. S., Cobianu, C., Buiu, O., Costea, S., Bostan, C., & Varachiu, N. (2010, October). Selection of gas sensing materials using the Hard Soft Acid Base theory; application to Surface Acoustic Wave CO 2 detection. In *C.A.S. 2010 Proceedings (International Semiconductor Conference)* (Vol. 1, pp. 247-250). IEEE.
58. Serban, B. C., Brezeanu, M., Cobianu, C., Costea, S., Buiu, O., Stratulat, A., & Varachiu, N. (2014, October). Materials selection for gas sensing. An HSAB perspective. In *2014 International Semiconductor Conference (C.A.S.)* (pp. 21-30). IEEE.